International Scholarly Research Network
ISRN Condensed Matter Physics
Volume 2012, Article ID 750497, 8 pages
doi:10.5402/2012/750497

Research Article

Characterization and Electrical Properties of $[C_6H_9N_2]_2CuCl_4$ Compound

M. Hamdi, A. Oueslati, I. Chaabane, and F. Hlel

Laboratoire de l'État Solide, Faculté des Sciences de Sfax, BP 1171, 3000 Sfax, Tunisia

Correspondence should be addressed to I. Chaabane, chaabane.iskandar@gmail.com

Received 31 October 2012; Accepted 24 November 2012

Academic Editors: M. Higuchi, A. N. Kocharian, V. Kochereshko, and M. Naito

We report measurements of X-ray powder diffraction, vibrational study, the differential scanning calorimetry (DSC), and the electric properties of a made-up $[C_6H_9N_2]_2CuCl_4$ sample. The alternative current (ac) conductivity of the compound $[C_6H_9N_2]_2CuCl_4$ has been measured in the temperature range 356–398 K and the frequency range 209 Hz–5 MHz. The Cole-Cole (the imaginer part (Z'') versus real part (Z') of impedance complex) plots are well fitted to an equivalent circuit model which consists of a parallel combination of a bulk resistance (R) and constant phase elements (CPE). The single semicircle indicates only one primary mechanism for the electrical conduction within $[C_6H_9N_2]_2CuCl_4$. The variation of the value of these elements with temperatures confirmed the result detected by DSC and dielectric measurements. Thus the conduction in the material is probably due to a hopping or a small polaron tunneling process.

1. Introduction

Organic-inorganic hybrid compounds can be designed to utilize synergistic interactions between the dissimilar components, which can yield new properties and/or an enhanced performance. Indeed, synergy will be critical in achieving targeted physical properties (e.g., electronic, optical and transport properties). Thus, organic-inorganic hybrid materials combine the advantageous properties characteristic of inorganic solids (e.g., high carrier mobilities, thermal stability) with those of organic molecules (e.g., ease of processing, high fluorescence efficiency, and large polarizability) [1–11]. A novel group of crystals, containing heteroaromatic cations like, pyridinium, substituted pyridinium, and imidazolium ones, have been recently synthesized and characterized [11–13]. Since aromatic heterocyclic cations are bestowed a significant electric dipole moment; thus some halogenoantimonates(III) and halogenobismuthates(III) containing these cations form strongly polar structures. Inorganic component can introduce some special structural units, such as distorted tetrahedron and octahedron. In an attempt to study the electric behavior in this class of compounds we have successfully synthesized a compound of formula bis(2-amino-4-methylpyridinium) tetrachloridocuprate(II) ($[C_6H_9N_2]_2[CuCl_4]$). At room temperature, the synthesized compound crystallizes in the monoclinic system (C2/c space group) with $Z = 4$ and the following unit cell dimensions: $a = 11.313\,(3)$ Å, $b = 12.272\,(3)$ Å, $c = 14.264\,(4)$ Å, and $\beta = 113.201\,(17)^\circ$ [11]. The crystal structure contains chains of cations $C_6H_9N_2^+$ alternating with stacks of tetrahedra anions of tetrachloridocuprate $CuCl_4^{2-}$ (Figure 1(a)). Both N–H$\cdots$Cl and π-π stacking interactions cause the formation of a three-dimensional supramolecular architecture.

(i) The bonding between inorganic and organic layer is established by four different hydrogen bonds ([N1–H1A$\cdots$(Cl1,Cl2i), N2–H2A$\cdots$Cl1, and N2–H2B$\cdots$Cl2ii). The N$\cdots$Cl distances vary between 3.294 (6) and 3.359 (6) Å. These interactions and the symmetrically related ones connect the anion to four surrounding cations (Figure 1(b)).

(ii) The cations interact via offset face-to-face, π-π stacking interactions leading to chains along the crystallographic c axis (Figure 1(c)) [11].

In the present paper we report the synthesis, X-ray powder diffraction patterns, DSC, infrared, Raman,

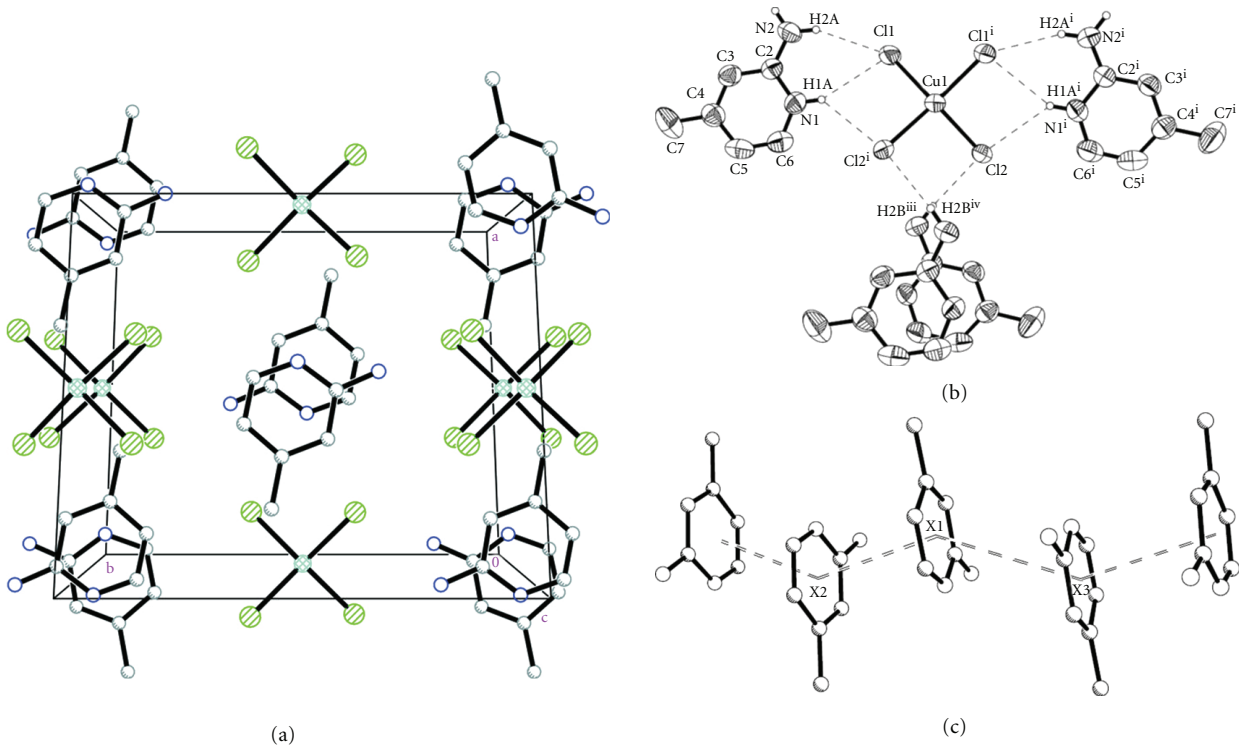

Figure 1: (a) Crystal packing diagram showing alternating stacks of anions and chains of cations. (b) The structure of the title compound, viewed down *c*. N–H· · · Cl–Cu intermolecular interactions are shown as dashed lines. (c) Cationic chains along the crystallographic *c* axis, assembled via offset face-to-face (π-π stacking; double broken lines) motifs.

and impedance spectroscopy characterizations of the $[C_6H_9N_2]_2CuCl_4$ compound.

2. Experimental

$[C_6H_9N_2]_2CuCl_4$ sample was prepared by mixing $CuCl_2$ (purity 98%; FLUKA), dissolved in hydrochloric acid solution (1 M), and the organic compound bis(2-amino-4-methylpyridinium) (purity 99%; FLUKA), in molar ratio 1 : 2. After six days, crystalline samples were obtained by slow evaporation at room temperature.

Schematically the reaction proposed in order to justify the obtaining $[C_6H_9N_2]_2CuCl_4$ sample is shown in the following equation:

$$2 \cdot [C_6H_8N_2] + CuCl_2 \xrightarrow{\text{HCl (1 M)}} [C_6H_8N_2]_2CuCl_4. \quad (1)$$

Powder X-ray diffraction was carried out initially to confirm the presence of the $[C_6H_9N_2]_2CuCl_4$ compound. A Siemens D500 was employed, using CuK_α radiation. A scanning rate of $0.028^\circ\ s^{-1}$ was employed.

Differential scanning calorimetry analysis was performed using a DSC NETZSCH 204 between 220 and 475 K at the heating rate of 5 K/min.

The infrared spectrum was recorded in the 400–4000 cm^{-1} range with a JASCO FT-IR 420 1000 spectrometer using samples pressed in spectroscopically pure KBr pellets.

The Raman spectrum of $[C_6H_9N_2]_2CuCl_4$ sample is recorded on a Kaiser Optical System spectrometer model-Hololab 5000R in the region 80–2000 cm^{-1} at room temperature.

The pellets of $[C_6H_9N_2]_2CuCl_4$ sample were prepared (diameter 8 mm; thickness 0.6 mm) by compressing the powder in a die using a hydraulic press at a pressure of 3000 kg/cm^2. The samples of the appropriate shape were sandwiched between two silver electrodes of the configuration Ag/electrolyte/Ag. The ac impedance data, $|Z|$, and phase angle were obtained in the frequency range 209 Hz–5 MHz using TEGAM 3550 impedance analyzer over the temperature range 356–398 K.

3. Results and Discussion

3.1. X-Ray Powder Diffraction Patterns. The room temperature X-Ray diffraction pattern of $[C_6H_9N_2]_2CuCl_4$ is shown in Figure 2. Lattice parameters were calculated with reference to the single-crystal X-ray study of bis(2-amino-4-methylpyridinium) tetrachloridocuprate(II) and using a computer program package Celref 2 based on the least square refinement method. The refined, in the monoclinic system (C2/c space group), of observed interplanar spacing *d*-values from the diffractograms show that refined lattice parameters are $a = 11.26\ (2)$ Å, $b = 12.22\ (2)$ Å, $c = 14.25\ (4)$ Å, and $\beta = 113.47\ (3)^\circ$. From these, it is found that $[C_6H_9N_2]_2CuCl_4$ is in a good agreement with the literature values [11].

3.2. Infrared and Raman Vibrational Study. Figures 3(a) and 3(b) show infrared (IR) and Raman spectra, respectively, of

Table 1: Infrared and Raman spectral data (cm^{-1}) and band assignments for $[C_6H_9N_2]_2[CuCl_4]$ sample.

IR wavenumbers (cm^{-1})	Raman wavenumbers (cm^{-1})	Assignments
	81	$\nu_2[CuCl_4]^{2-}$
	135	ν_4 $[CuCl_4]^{2-}$
	180	
	223	$\nu_3[CuCl_4]^{2-}$
	279	
428	430	τ C=C
512		N=C–N
572	565	δ NH
	590	
718		Torsion of the cycle
	762	
840		
860		ρ CH
	940	
962	961	
984	989	
1036		C–C
1180	1179	δ CH_3
1224	1224	ν C–N
1300	1297	δ (CH) + δ (NH) and ν (CN)
1436	1416	
1482	1484	ν (C–C), δ (CH) and δ (NH)
1528		
1624		ν C=C
1658		
2361		ν CH (−)
2956		ν CH
3010		ν CH (+)
3094		
3166		ν_{as} NH (−)
3188		ν_{as} NH_2
3226		
3296		ν_s NH_2
3366		
3732		ν_{as} NH (+)

ν_2: bending, ν_3: asymmetric stretching, ν_4: asymmetric bending, ν: stretching, ρ: rocking, δ: deformation, τ: torsion, (−): out of plane, (+): in plane.

the reported compound at room temperature. A detailed assignment of all the bands is difficult, but we can attribute some of them by comparison with similar compounds [12–15]. The assignments are listed in Table 1.

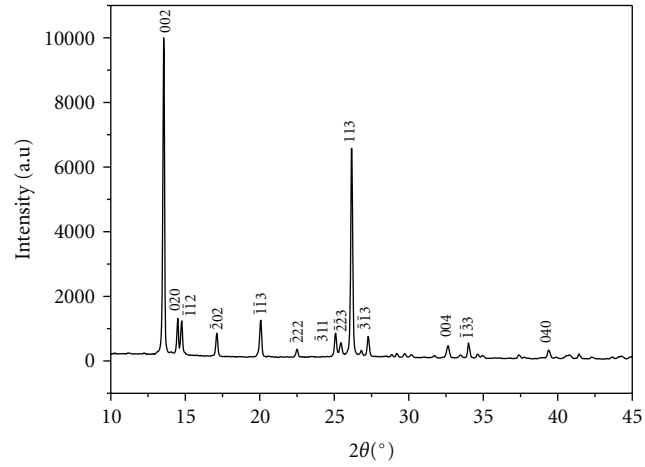

Figure 2: X-ray diffractogram of $[C_6H_9N_2]_2CuCl_4$ compound.

The principal bands are assigned to the internal modes of organic cation. The C=C bands exhibit torsion vibration at 425 cm^{-1} in IR and 430 cm^{-1} in Raman the stretching vibration appears at 1624 and 1658 cm^{-1} in IR. The bands observed at 762, 940, 961, 989 and 840, 860, 962, and 984 cm^{-1} in Raman and IR, respectively, are attributed to CH wagging modes. The CH stretching vibrations are observed at 2362, 2956, and 3010 cm^{-1} in IR. The bands observed at 3094 and 3166 cm^{-1} in IR are associated to the asymmetric NH stretching out of plane those observed at 3366 and 3732 cm^{-1} in IR are ascribed to asymmetric NH stretching in plane.

A free $CuCl_4^{2-}$ ion under T_d symmetry has four fundamental vibrations the symmetric stretching mode ν_1, the bending mode ν_2 observed at 77 cm^{-1}. The average frequencies observed at 267, 248 and 136, 118 cm^{-1} are ascribed to the asymmetric stretching mode ν_3 and asymmetric bending mode ν_4, respectively. All the modes are Raman active, whereas only ν_3 and ν_4 are active in the IR [16]. Meanwhile, the vibrations of the $CuCl_4^{2-}$ in this structure are shown in Raman spectra. The ν_2 mode appears as one strong band at 81 cm^{-1}. The ν_3 mode appears as one strong band at 279 cm^{-1} and one shoulder at 223 cm^{-1}. The ν_4 mode is observed as one strong band at 180 and one shoulder at 135 cm^{-1}. The higher frequency value obtained for the ν_2, ν_3, and ν_4 modes than those in a free $CuCl_4^{2-}$ ion confirms the distortion of $CuCl_4$ tetrahedra as is evident from different Cu–Cl bond lengths determined by the X-ray diffraction study [11]. The presence of hydrogen bonds and Jahn-Teller effect may be the reason for the observed distortion in the $CuCl_4$ tetrahedra in this structure [11].

The infrared and Raman studies confirm the presence of the organic group $C_6H_9N_2$ and the tetrahedral anion $CuCl_4^{2-}$.

3.3. D.S.C Analysis. Results of differential scanning calorimetry measurements, recorded in the temperature range 220–475 K, are presented in the thermogram shown in Figure 4.

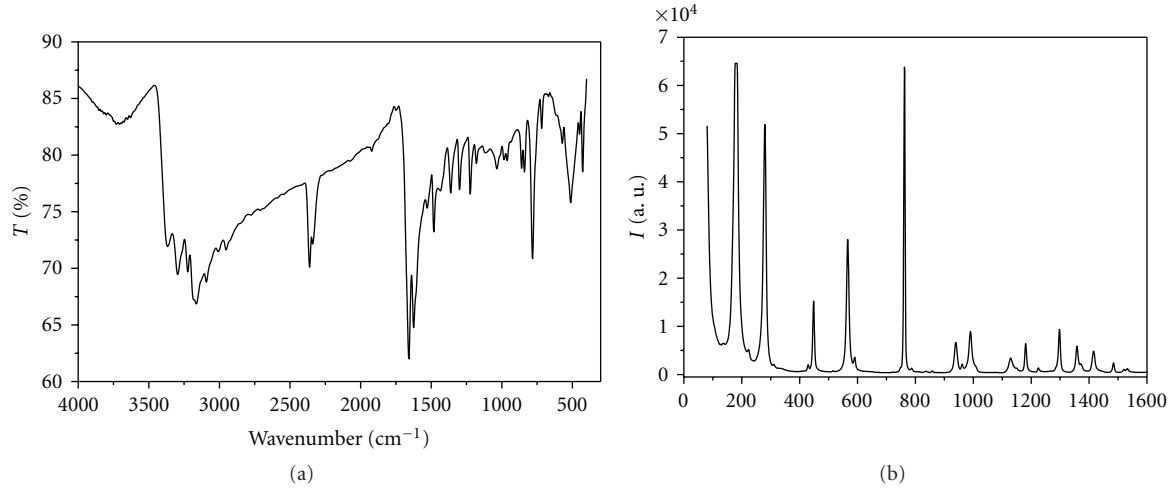

Figure 3: (a) Infrared spectrum of $[C_6H_9N_2]_2CuCl_4$, (b) Raman spectrum of $[C_6H_9N_2]_2CuCl_4$ compound.

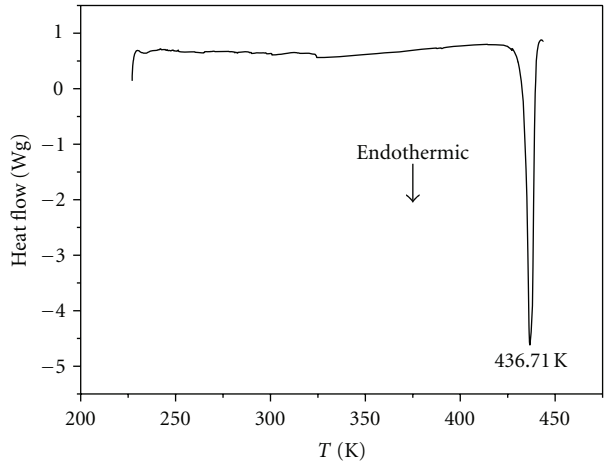

Figure 4: Differential scanning calorimetry of $[C_6H_9N_2]_2CuCl_4$ sample.

It shows the presence of an endothermic peak located at 436.71 K corresponding to the fusion of the compound $[C_6H_9N_2]_2CuCl_4$.

3.4. Electrical Properties. Complex impedance spectroscopies have been used to study electrical properties of the $[C_6H_9N_2]_2CuCl_4$ compound. It is useful for analyzing the electrical processes occurring in a compound on the application of a small ac signal as input perturbation. In our case the resultant response (when plotted in a complex plane shown in Figures 5(a) and 5(b)) appears in the form of depressed semicircles. The observed depressed semicircles can usually be reproduced with an equivalent circuit formed by parallel combination of resistance polarization (R_p) and constant phase elements (CPEs) [2]. Usually Z_{CPE} ($Z_{CPE} = 1/A_0(j\omega)^{\alpha}$) is considered to be a dispersive capacitance. α is the measure of the capacitive nature of the element: if $\alpha = 1$ the element is an ideal capacitor, if $\alpha = 0$ it behaves as a frequency independent ohmic resistor, whereas if $\alpha = -1$ it behaves as an inductance.

The impedance of the equivalent circuit shown in Figure 6 can be expressed as follows: $Z = Z' - jZ''$ where

$$Z' = \frac{R_p\left(1 + R_pA_0\omega^{\alpha}\cos(\alpha\pi/2)\right)}{\left(1 + R_pA_0\omega^{\alpha}\cos(\alpha\pi/2)\right)^2 + \left(R_pA_0\omega^{\alpha}\sin(\alpha\pi/2)\right)^2}, \quad (2)$$

$$-Z'' = \frac{R_p^2A_0\omega^{\alpha}\sin(\alpha\pi/2)}{\left(1 + R_pA_0\omega^{\alpha}\cos(\alpha\pi/2)\right)^2 + \left(R_pA_0\omega^{\alpha}\sin(\alpha\pi/2)\right)^2}. \quad (3)$$

The curves of Z' and $-Z''$ versus frequency at several temperatures are fitted by (2) and (3), respectively. In Figures 7(a) and 7(b) are represented Z' and $-Z''$ versus frequency at 381 K, respectively, together with fits to the equivalent circuit presented in Figure 6. All fitted curves at each temperature show the good conformity of calculated lines with the experimental data indicating that the suggested equivalent circuit describes the crystal-electrolyte interface reasonably well.

The resistance R_p, the capacitance A_0, and α have been simulated using a mean square method which consists to minimize the difference between the experimental and calculate data. The values of the equivalent circuit elements have been listed in Table 2.

The temperature dependences of the fitted parameters α ($0.72 < \alpha < 0.81$) show that the constant phase elements (CPEs) represent a leaking (nonideal) capacitor as it contains both imaginary and real parts and constitute energy dissipation because of the presence of the impedance real part.

The capacitance values (A_0) of the equivalent circuit element are critical to the identification of the grain boundary and grain interior contribution. It has already been established in the literature that the dispersion in the boundaries and in the grain bulk interior has a capacitance value in the range of nF and pF, respectively, [17–20]. In our

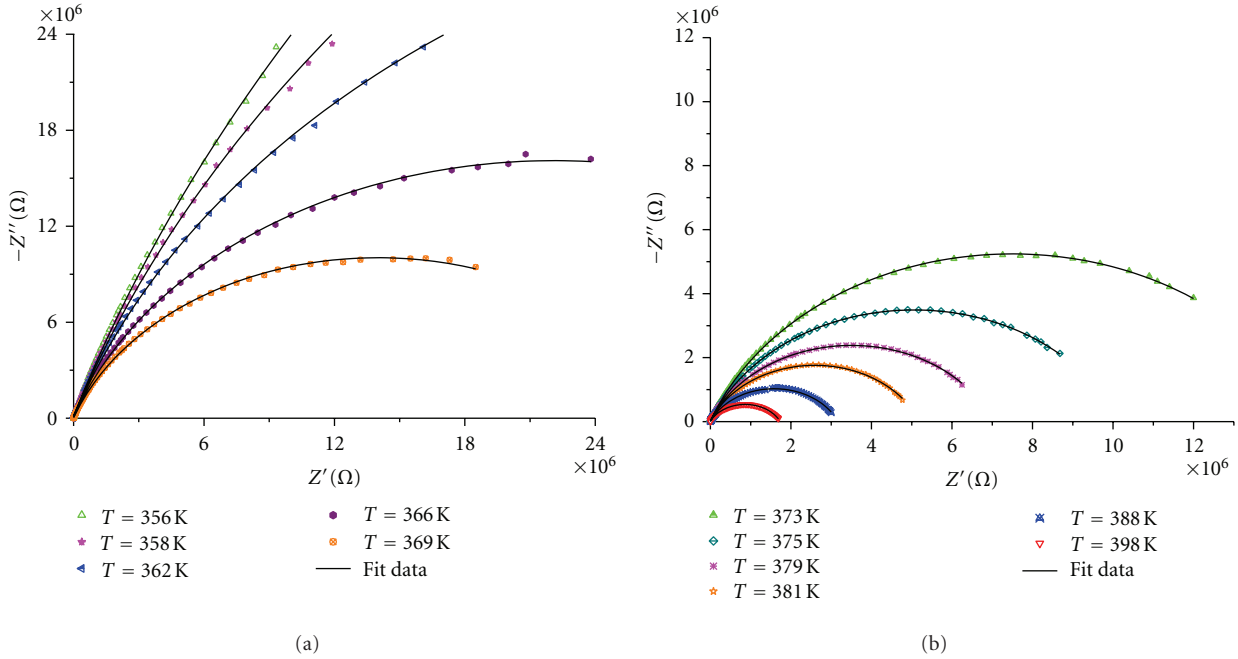

Figure 5: (a), (b) Impedance spectra of $[C_6H_9N_2]_2CuCl_4$ sample at different temperature ranges.

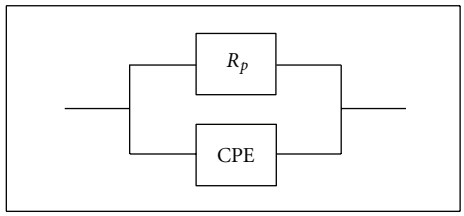

Figure 6: Equivalent circuit model of $[C_6H_9N_2]_2CuCl_4$ sample.

Table 2: Equivalent circuit parameters obtained at some temperatures.

T (K)	R_p (10^6 Ω)	A_0 (10^{-12} F)	α
356	100.37	50.584	0.816
358	103.36	51.548	0.812
362	68.36	50.615	0.819
366	41.46	61.505	0.806
369	27.17	72.764	0.798
373	14.97	94.271	0.783
375	10.18	114.14	0.773
379	7.06	132.9	0.765
381	5.24	142.07	0.764
388	3.19	173.71	0.751
398	1.74	234.86	0.729

case the capacitance values (A_0) vary between 50.584 pF and 234.86 pF in the temperature range 356 K–398 K. This implies that the single semicircular response is from grain interiors, which is expected from the sample where no grain boundaries are involved.

Knowing the bulk resistance, obtained from equivalent circuit parameter values, and the dimensions of the sample, the conductivity (σ_{dc}) has been calculated at each temperature by means of the relation:

$$\sigma_{dc} = \frac{e}{R_p S}, \tag{4}$$

where e/S represents the sample geometrical ratio. The temperature dependence of the conductivity is represented in the form of $\log(\sigma_{dc}T)$ versus 1000/T plot in Figure 8. An Arrhenius type behaviour, $\sigma_{dc}T = B\exp(-E/k_\beta T)$, is shown in the temperature range $355\,K < T < 400$ K, where σ_{dc} is the dc conductivity at temperature T, B the preexponential factor, K_β the Boltzmann's constant, and E is the thermal activation energy for the ion migration. The activation energies obtained from the slopes of $[C_6H_9N_2]_2CuCl_4$ sample are Ea = 1.347 eV. The variation of electrical conductivity versus the angular frequency of $[C_6H_9N_2]_2CuCl_4$ sample at various temperatures is plotted in Figure 9. The electric response of the low conductivity materials is usually characterized by the well-known universal dynamic response [21]. Consider

$$\sigma_{ac} = \sigma_{dc} + A\omega^n, \tag{5}$$

where σ_{dc} is the dc conductivity in the particular range of temperature, A is a temperature dependent parameter, and n is the temperature-dependent exponent in the range of $0 \le n \le 1$ [21–23]. The exponent n represents the degree of interaction between mobile ions with the lattices around them and the prefactor exponent A determines the strength of polarizability.

In order to explain the behaviour of σ with both frequency and temperature, different theoretical models have

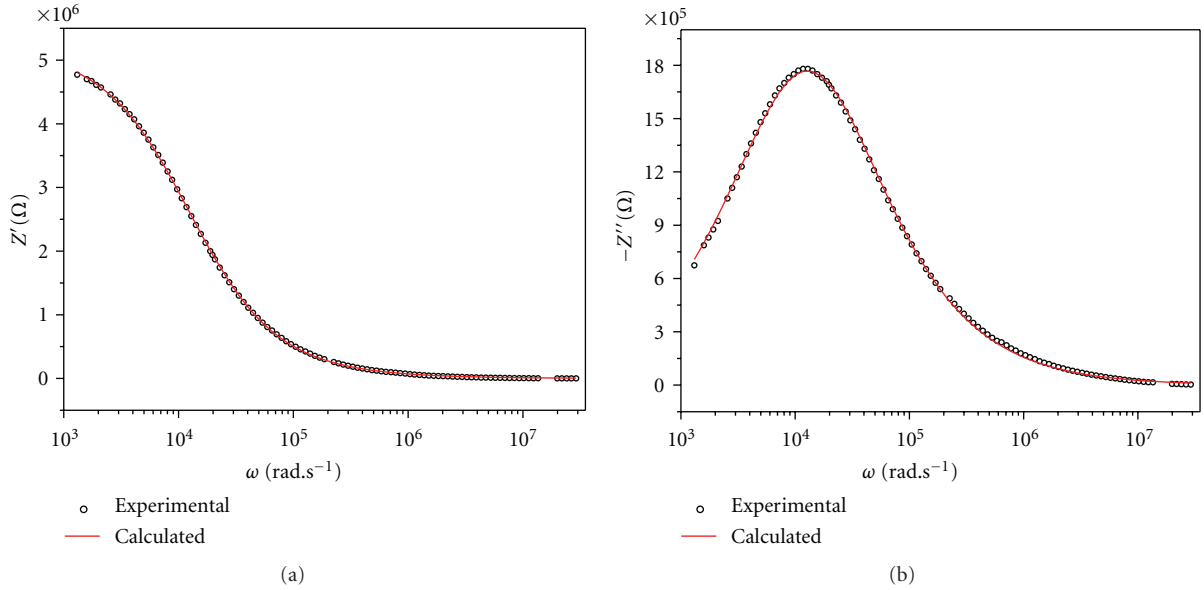

Figure 7: (a), (b) Experimental plot fitted with the corresponding electrical equivalent model of Z' and Z'', respectively, with frequency ($T = 381$ K). circles and line represent the experimental and fitted data, respectively.

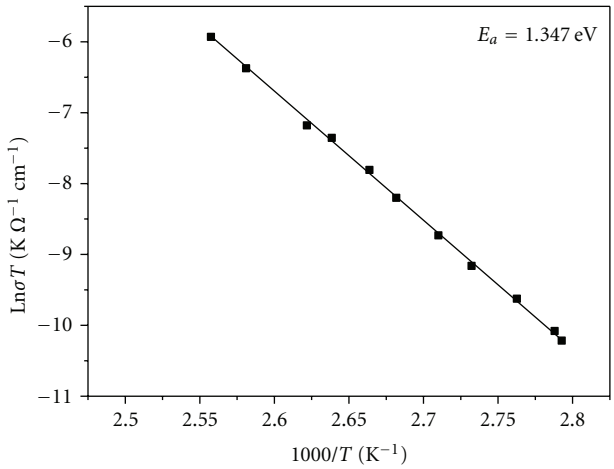

Figure 8: Temperature dependence of $\ln(\sigma \cdot T)$.

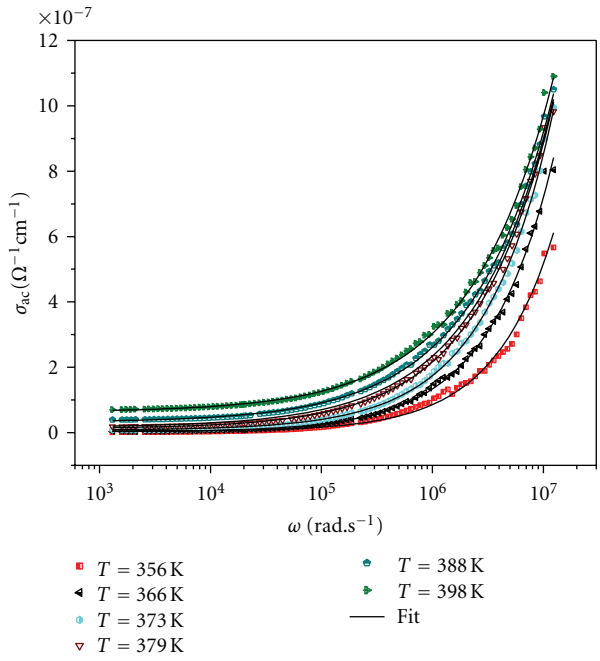

Figure 9: Frequency dependence of the ac conductivity at various temperatures.

been proposed to correlate the conduction mechanism of AC conductivity with $n(T)$ behaviour. According to quantum mechanical tunneling model [22, 24, 25], the exponent n is temperature independent. The large overlapping polaron model [25] predicted that n decreases with increasing temperature up to a certain temperature degree, after which, it begins to increase with further rise in temperature. The small polaron tunneling model and the classical hopping model over a barrier separating two sites [26] predicted that n decreases with increasing the temperature.

The temperature dependence on the fitted frequency exponent n is shown in Figure 10. The n values decreases with increasing the temperature. Comparing our results of $n(T)$ shown in Figure 10 with the abovementioned models, it can be concluded that the classical hopping or small polaron tunneling model is the most probable conduction mechanism for the $[C_6H_9N_2]_2CuCl_4$ crystal.

4. Conclusions

The diffraction of X-rays powder shows that the compound $[C_6H_9N_2]_2CuCl_4$ crystallizes in the monoclinic system (space group C2/c, $Z = 4$) with the following unit cell

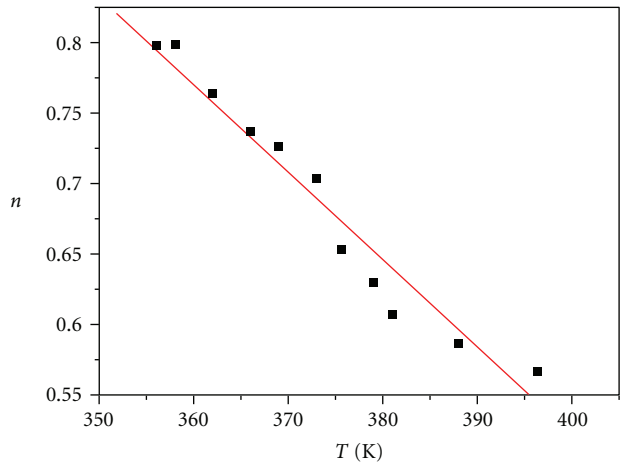

Figure 10: Temperature dependence of the frequency exponent n.

dimensions: $a = 11.26\ (2)$ Å, $b = 12.22\ (2)$ Å, $c = 14.25\ (4)$ Å, and $\beta = 113.47\ (3)^\circ$, similar of the X-ray diffraction data collection described by Al-Far and Ali.

The differential calorimetric analysis shows the presence of only one endothermic peak located at 436.71 K which corresponds to the fusion of material. The analysis by infrared and Raman spectroscopy made it possible to check the presence of the functional groupings, of the ionic groupings of material.

The analysis of the frequency dispersion of the real imaginary components of the complex impedance allowed us to determine an equivalent electrical circuit for the electrochemical cell with $[C_6H_9N_2]_2CuCl_4$. The variations of the values of elements of this equivalent circuit with temperature confirmed the result detected by DSC and dielectric measurements. The temperature dependence of conductivity was analyzed using the Arrhenius approach.

The AC conductivity is analyzed by Jonscher's law, and suggests that the classical hopping or small polaron tunneling model is the most probable conduction mechanism for the $[C_6H_9N_2]_2CuCl_4$ crystal.

References

[1] I. Chaabane, F. Hlel, and K. Guidara, "Dielectric spectroscopy study of the new compound $[C_{12}H_{17}N_2]_2CdCl_4$," *Ionics*, vol. 16, no. 4, pp. 371–377, 2010.

[2] I. Chaabane, F. Hlel, and K. Guidara, "Electrical study by impedance spectroscopy of the new compound $[C_{12}H_{17}N_2]_2CdCl_4$," *Journal of Alloys and Compounds*, vol. 461, no. 1-2, pp. 495–500, 2008.

[3] I. Chaabane, F. Hlel, and K. Guidara, "Synthesis, Infra-red, Raman, NMR and structural characterization by X-ray Diffraction of $[C_{12}H_{17}N_2]_2CdCl_4$ and $[C_6H_{10}N_2]_2Cd_3Cl_{10}$ compounds," *Journal of PMC Physics B*, vol. 1, article 11, 2008.

[4] A. K. Vishwakarma, P. S. Ghalsasi, A. Navamoney, Y. Lan, and A. K. Powell, "Structural phase transition and magnetic properties of layered organic-inorganic hybrid compounds: P-Haloanilinium tetrachlorocuparate(II)," *Polyhedron*, vol. 30, no. 9, pp. 1565–1570, 2011.

[5] K. Shibuya, M. Koshimizu, Y. Takeoka, and K. Asai, "Scintillation properties of $(C_6H_{13}NH_3)_2PbI_4$: exciton luminescence of an organic/inorganic multiple quantum well structure compound induced by 2.0 MeV protons," *Nuclear Instruments and Methods in Physics Research B*, vol. 194, no. 2, pp. 207–212, 2002.

[6] P. Ren, J. Qin, T. Liu, and S. Zhang, "Synthesis, structure and second harmonic generation of novel inorganic-organic hybrid, $(p$-cyano-1-hydrogenpyridinium$)_2CdI_4$," *Inorganic Chemistry Communications*, vol. 7, no. 1, pp. 134–136, 2004.

[7] Y. Liu, P. Yang, and J. Meng, "Synthesis, crystal structure and optical properties of a novel organic inorganic hybrid materials $(C_9H_{14}N)_2PbCl_4$," *Solid State Sciences*, vol. 13, no. 5, pp. 1036–1040, 2011.

[8] P. S. Ghalsasi and K. Inoue, "Distorted perovskite structured organic-inorganic hybrid compounds for possible multiferroic behavior: $[$n-alkyl$]_2FeCl_4$," *Polyhedron*, vol. 28, no. 9-10, pp. 1864–1867, 2009.

[9] N. Kitazawa, M. Aono, and Y. Watanabe, "Excitons in organic-inorganic hybrid compounds $(C_nH_{2n+1}NH_3)2PbBr4$ (n = 4, 5, 7 and 12)," *Thin Solid Films*, vol. 518, no. 12, pp. 3199–3203, 2010.

[10] T. J. Coffey, C. P. Landee, W. T. Robinson, M. M. Turnbull, M. Winn, and F. M. Woodward, "Transition metal halide salts of 2-amino-3-methylpyridine: Synthesis, crystal structures and magnetic properties of (3-MAP)2CuX4 [3-MAP = 2-amino-3-methylpyridinium; X = Cl, Br]," *Inorganica Chimica Acta*, vol. 303, no. 1, pp. 54–60, 2000.

[11] R. H. Al-Far and B. F. Ali, "Bis(2, 6-dimethyl pyridinium) tetra bromido zincate(II)," *Acta Crystallographica Section E*, vol. 65, pp. 581–582, 2009.

[12] A. K. Rai, R. Singh, K. N. Singh, and V. B. Singh, "FTIR, Raman spectra and ab initio calculations of 2-mercaptobenzothiazole," *Spectro Chimica Acta A*, vol. 63, no. 2, pp. 483–490, 2006.

[13] M. N. Ohnet, M. Jouan, G. Ménard et al., "Chemical bonding in metal-heterocumulene complexes. Part 3. Vibrational study of the cyanamide ligand NCNR2 and the complexes $(CO)_5MNCNR_2$ (M is Cr or W; R is C_2H_5 or CH_3), and determination of the force field for the complex $(CO)_5CrNCN(C_2H_5)_2$," *Spectrochimica Acta A*, vol. 52, no. 5, pp. 505–526, 1996.

[14] L. A. Sheludyakova and T. V. Basova, "Hexachlorocuprate(II) anion: vibration spectra and structure," *Journal of Structural Chemistry*, vol. 43, no. 1, pp. 581–586, 2002.

[15] T. Guerfel and A. Jouini, "Crystal structure, thermal analysis, and IR spectroscopic investigation of bis(2-amino-6-methyl) pyridinium sulfate," *Journal of Chemical Crystallography*, vol. 35, no. 7, pp. 513–521, 2005.

[16] A. Oueslati, F. Hlel, and M. Gargouri, "Preparation and characterization of organic inorganic hybrid compound $[N(C_4H_9)_4]_2Cu_2Cl_6$," *Ionics*, vol. 10, p. 11581, 2010.

[17] K. S. Rao, P. M. Krishna, D. M. Prasad, J. H. Lee, and J. S. Kim, "Electrical, electromechanical and structural studies of lead potassium samarium niobate ceramics," *Journal of Alloys and Compounds*, vol. 464, no. 1-2, pp. 497–507, 2008.

[18] J. C. M'Peko, D. L. Spavieri, and M. F. de Souza, "In situ characterization of the grain and grain-boundary electrical responses of zirconia ceramics under uniaxial compressive stresses," *Applied Physics Letters*, vol. 81, no. 18, pp. 2827–2832, 2002.

[19] A. Huanosta, O. A. Fregoso, E. Amano, C. T. Muñoz, M. E. M. Alvarez, and J. G. M. Alvarez, "ac impedance analysis on crystalline layered and polycrystalline bismuth titanate," *Journal of Applied Physics*, vol. 69, no. 1, pp. 404–408, 1991.

[20] H. Ye, C. Q. Sun, H. Huang, and P. Hing, "Dielectric transition of nanostructured diamond films," *Applied Physics Letters*, vol. 78, no. 13, pp. 1826–1828, 2001.
[21] R. M. Hill and A. K. Jonscher, "DC and AC conductivity in hopping electronic systems," *Journal of Non-Crystalline Solids*, vol. 32, no. 1-3, pp. 53–69, 1979.
[22] N. F. Mott and E. A. Davis, *Electronic Processes in Non-Crystalline Materials*, Clarendon Press, Oxford, UK, 2nd edition, 1979.
[23] R. H. Chen, R. Y. Chang, and S. C. Shern, "Dielectric and AC ionic conductivity investigations in $K3H(SeO_4)_2$ single crystal," *Journal of Physics and Chemistry of Solids*, vol. 63, no. 11, pp. 2069–2077, 2002.
[24] A. Oueslati, F. Hlel, K. Guidara, and M. Gargouri, "AC conductivity analysis and dielectric relaxation behavior of $[N(C_3H_7)_4]_2Cu_2Cl_6$," *Journal of Alloys and Compounds*, vol. 492, no. 1-2, pp. 508–514, 2010.
[25] A. R. Long, "Frequency-dependent loss in amorphous semiconductors," *Advances in Physics*, vol. 31, pp. 553–637, 1982.
[26] S. R. Elliott, "A. c. Conduction in amorphous chalcogenide and pnictide semiconductors," *Advances in Physics*, vol. 36, no. 2, pp. 135–218, 1987.